Journal of Biomedical Optics

BiomedicalOptics.SPIEDigitalLibrary.org

Fast spectral surface plasmon resonance imaging sensor for real-time high-throughput detection of biomolecular interactions

Kaiqiang Chen
Youjun Zeng
Lei Wang
Dayong Gu
Jianan He
Shu-Yuen Wu
Ho-Pui Ho
Xuejin Li
Junle Qu
Bruce Zhi Gao
Yonghong Shao

SPIE.

Kaiqiang Chen, Youjun Zeng, Lei Wang, Dayong Gu, Jianan He, Shu-Yuen Wu, Ho-Pui Ho, Xuejin Li, Junle Qu, Bruce Zhi Gao, Yonghong Shao, "Fast spectral surface plasmon resonance imaging sensor for real-time high-throughput detection of biomolecular interactions," *J. Biomed. Opt.* **21**(12), 127003 (2016), doi: 10.1117/1.JBO.21.12.127003.

Fast spectral surface plasmon resonance imaging sensor for real-time high-throughput detection of biomolecular interactions

Kaiqiang Chen,[a,†] Youjun Zeng,[a,†] Lei Wang,[a,†] Dayong Gu,[b] Jianan He,[b] Shu-Yuen Wu,[c] Ho-Pui Ho,[c] Xuejin Li,[a] Junle Qu,[a] Bruce Zhi Gao,[d] and Yonghong Shao[a,*]

[a]Shenzhen University, College of Optoelectronic Engineering, Key Laboratory of Optoelectronic Devices and Systems of Ministry of Education and Guangdong Province, Shenzhen Key Laboratory of Sensor Technology, Shenzhen 518060, China
[b]Shenzhen Entry-Exit Inspection and Quarantine Bureau, Shenzhen 518033, China
[c]Chinese University of Hong Kong, Department of Electronic Engineering, Shatin, NT, Hong Kong
[d]Clemson University, Department of Bioengineering and COMSET, Clemson, South Carolina 29634, United States

Abstract. A fast surface plasmon resonance (SPR) imaging biosensor system based on wavelength interrogation using a liquid crystal tunable filter (LCTF) is presented. The system combines the merits of wide-dynamic detection range offered by the spectral approach and multiplexed high-throughput data collection with a two-dimensional (2-D) biosensor array. The key feature of the reported scheme is a feedback loop that drives the LCTF to achieve fast tracking of the SPR dip movement caused by the binding of target molecules to the sensor surface. Experimental results show that the system is capable of completing an SPR dip measurement within 4 s. Based on using a spectral window of about 100 nm, the experimental dynamic detection range and refractive index resolution are 4.63×10^{-2} RIU and 5.87×10^{-6} RIU, respectively. As also demonstrated herein using 2-D microsensor arrays, among the spectral SPR sensors, the reported system is most suitable for multiplexed label-free biosensing applications. [DOI: 10.1117/1.JBO.21.12.127003]

Keywords: surface plasmon resonance; surface plasmon resonance imaging; microarray analysis; biosensor; liquid crystal tunable filter.

Paper 160615R received Sep. 3, 2016; accepted for publication Nov. 18, 2016; published online Dec. 9, 2016.

1 Introduction

Surface plasmon resonance (SPR) biosensors, which offer unique real-time and label-free measurement capabilities with high detection sensitivity, have become an important tool for exploring the kinetics of biomolecular interactions and have been widely adopted in detection of chemical and biological analytes.[1–4] Moreover, by combining the SPR approach with an imaging system, we can readily achieve high-throughput real-time label-free biosensing in two-dimensional (2-D) microarrays and parallel monitoring of multiple biomolecular interactions.[5–9] If the issues related to data-capture speed and detection sensitivity can be adequately resolved, the SPR imaging approach may become a candidate to replace the well-established fluorescence-based microarray technique, which is hobbled by photobleaching and lack of quantitative information.

The SPR phenomenon produces a minimum in the reflectivity, called the SPR dip, because the incident p-polarized light resonantly couples with a surface plasma wave at a specific angle or wavelength. The resonant coupling occurs when

$$k_x = \frac{2\pi n_p}{\lambda}\sin\theta \approx \frac{2\pi}{\lambda}\sqrt{\frac{\varepsilon_{mr} n_s^2}{\varepsilon_{mr} + n_s^2}} = k_{sp},$$

where n_p is the refractive index (RI) of the prism, λ is the wavelength of the excitation light, ε_{mr} is the real part of a complex dielectric constant of Au, θ is the angle of incidence, and n_s is the RI of the sample at the metal/dielectric interface.[10]

The position of the SPR dip is very sensitive to changes in the RI of the sample at the metal/dielectric interface. Analyte binding onto the sensor surface will induce a change in the RI at the metal/dielectric interface, thus making it possible to detect the interactions between biological molecules in the vicinity of the metal/dielectric interface through tracking the location of the SPR dip. To accurately determine the position of the SPR dip, three approaches based on intensity, angle, and wavelength interrogations have been developed and widely reported. In the intensity measurement mode, which has the highest imaging speed, the shift of the SPR dip is translated into a change in reflectivity in the linear region of the SPR angular or spectral response curve. This requires both the incidence angle and the wavelength of excitation light to be fixed and optimized for the best possible resolution. However, these requirements severely restrict the choice of operating point and dynamic range over a large sensor surface area and the capacity to simultaneously perform detection of multiple interactions.[11]

In the angular interrogation mode, the shift of the SPR dip can be monitored by continuous scanning of the SPR angular spectrograph. Compared to the intensity measurement mode, the angular interrogation mode has a wider dynamic range of detection.[12] Continuous scanning of the incidence angle by mechanical means in typical angular interrogation-based SPR sensors is slow and usually requires quite complex mechanisms.

*Address all correspondence to: Yonghong Shao, E-mail: shaoyh@szu.edu.cn

†Equal contributors as first authors.

1083-3668/2016/$25.00 © 2016 SPIE

To overcome these shortcomings, several methods have been reported, including the use of a converging excitation beam,[13,14] one-dimensional (1-D) acousto-optical deflector scanner,[15] and controlled mirror scanning.[16] However, the angular interrogation-based SPR sensor is a compromise in terms of measurement range: the use of a fixed excitation wavelength can offer only the best SPR absorption characteristics within a narrow range of reflective index.

The wavelength interrogation-based SPR sensor is much more flexible: the user chooses a range of wavelengths and can select the best spectral window for obtaining the strongest SPR modulation depth.[6] Moreover, wavelength interrogation SPR is known to provide a wide dynamic range and the possibility of detection resolution similar to that offered by angle interrogation. In this interrogation mode, a broadband light is used and the SPR spectral profile can be obtained either by scanning the incidence wavelength or by using a spectrometer for analyzing the reflected beam.[17–20] If proper data acquisition and analysis schemes have been implemented, the spectrometer-based SPR sensor can provide fast detection of a single sensor site or even 1-D line arrays.[21,22] However, this is not a straightforward method for detecting 2-D arrays. Recently, the approach of scanning the incident wavelength has been realized through use of a rotating grating that acts as a fast monochromator.[17,23] To realize fast scanning of wavelength for spectral SPR imaging sensors, a nonmechanical liquid crystal tunable filter (LCTF) scanning technique in a fixed wide wavelength range (650 to 1100 nm or 480 to 720 nm) has been developed.[24] Large changes in RI may occur when the interaction time is long, analyte concentration levels are high, or the size of the target molecules is large. The spectral SPR sensing design typically sweeps continuously through a wide wavelength range to ensure that the SPR dip never moves out of the range of interest. Moreover, it usually takes ~2 s for monochromator scanning or 100-ms LCTF scanning to produce a data point on the SPR plot for each wavelength. The measurement time of the SPR dip may not be short enough to achieve real-time monitoring of binding interactions, thereby making it impossible to obtain a true picture of interaction kinetics. Therefore, the issue of achieving a fast scanning speed remains unresolved. To improve measurement speed, a special-fitting algorithm based on using five parameters has been developed for the wavelength interrogation SPR sensors.[8,11] The measurement time per SPR dip has been shortened dramatically to 10 s. In this paper, we present a novel fast wavelength-scanning SPR imaging scheme that contains no mechanical moving parts and automatically tracks the movement of the SPR dip using a feedback loop. With the use of an LCTF, the measurement time for an SPR dip is about 4 s, and any spectral range of choice can be scanned at high speed with a good degree of flexibility. To our knowledge, this is the fastest wavelength interrogation SPR imaging sensor ever reported in the literature. The measurement time can be further shortened by a large amount if we also implement the five-parameter fitting algorithms previously reported.[11]

2 Methods

2.1 *Experimental Setup*

Figure 1 shows a schematic of our experimental setup. Light from a 100-W halogen tungsten lamp is coupled to the inverted prism through a multimode optical fiber for SPR excitation. A bandpass filter selects an input wavelength window with a

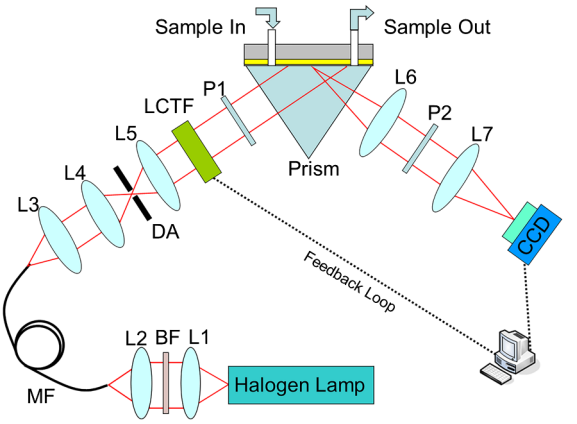

Fig. 1 Schematic of our SPRi system in the Kreschmann configuration. Light from a halogen lamp is collected by a multimode fiber through a set of coupling optics. At the exit end of the fiber, the beam is collimated by a group of lenses and spatially filtered by an aperture before passing through the tunable spectral filter unit and a linear polarizer. The sensor surface is imaged by a CCD camera using two imaging lenses. L_1 to L_7: lens; BF: bandpass filter; MF: multimode fiber; DA: diaphragm aperture; LCTF: liquid crystal tunable filter; P_1 and P_2: polarizer.

center wavelength of 610 nm and full width at half maximum (FWHM) of 220 nm. The LCTF rapidly scans the output wavelength in a stepwise manner. For our LCTF unit (VariSpec, VIS-10-20-STD), the FWHM, spectral tuning resolution, and response time are, respectively, 10 nm, 0.5 nm, and 50 ms. In our experiments, we chose a wavelength step of 1 nm as this was found to have the lowest level of noise in the final detected signal. While the Kretschmann configuration has been adopted, the SPR cell consists of an equilateral prism made of BK7 glass, a microscope glass slide coated with a 48-nm-thick gold film, and a flow chamber for sample injection. The incident angle can be manually set to an optimized value calculated using Fresnel equations. In the present case, the angle for pure water with an excited wavelength of 660 nm is 72.5 deg. The output light is captured by a 12-bit CCD camera. The A-D card (model number: NI DAQ 6259) generates a triggering signal that synchronizes the operation of the LCTF and CCD camera. An exposure time of 50 ms/wavelength is used because of the compromise between camera capture speed and signal-to-noise ratio. In our experiments, it takes 50 ms for the LCTF to switch the wavelength before the CCD starts its exposure cycle. Consequently, the CCD camera records a long series of images taken at different wavelengths within a prescribed spectral range. Figure 2 shows a series of recorded CCD image frames that covers the spectral dip as selected by the LCTF. Each pixel within the CCD image frame provides one wavelength data point within the spectral SPR profile of a small region in the sensor surface. Theoretically, this one-to-one correspondence between the sensor surface and the 2-D CCD imaging pixel arrays may offer massively parallel-biosensing capability. Upon analyzing a series of images, one can build a set of spectral plots that covers all the pixels within the sensor surface. Here, we use a common second order polynomial-fitting algorithm to locate the spectral dip, which corresponds to the resonant wavelength of each pixel. The data analysis procedures are performed in an automatic mode using lab-designed software based on numerical comparison techniques.

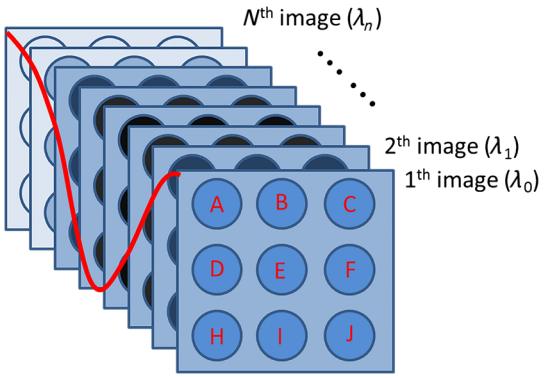

Fig. 2 Schematic of the image recording process. Regions marked by A-J represent the sample areas on the chip. First to *N*'th frame represent a series of images recorded by the CCD camera as we sweep the center wavelength of the LCTF step-by-step. The intensity values of each pixel location taken from the frames constitute one SPR spectral plot, as indicated by the red curve. Therefore, the number of pixels in each image frame corresponds to the number of spectral plots from the system.

2.2 *Feedback Loop*

The feedback loop shown in Fig. 1 is designed to automatically track the shift of the SPR dip caused by the binding of target biomolecules. Most importantly, incorporation of this feedback loop drastically reduces the spectral width one needs to sweep before hitting an SPR dip. For example, it takes 80 s to obtain the resonance dip with a traditional stepping monochromator based on a spectral range of 40 nm and a step-size of 1 nm, whereas with the help of a feedback loop, the time required by the present system to find the SPR dip is 4 s. Moreover, an LCTF can scan the incident wavelength across any spectral range according to an optimized strategy with minimal delay. Consequently, the amount of time required to arrive at an SPR resonance data point is significantly shorter.

Figure 3 schematically shows how the feedback loop operates. First, an initial SPR spectral profile is obtained by scanning the incident wavelength across a large spectral range to extract the baseline resonant wavelength λ_0. Then a spectral range $\lambda_0 - x$ to $\lambda_0 + x$ is chosen. With this, the desired SPR dip with sufficient resolution (<0.01 nm) (solid red straight line along horizontal axis in which x is half the width of the wavelength-scanned range) can be obtained.[25] The corresponding partial SPR plot near the SPR dip (red dotted curve) is repeated if the RI n_0 of the baseline solution does not change. When a change of RI has taken place, e.g., from n_0 to n_1, a new partial SPR plot (solid red curve) is obtained by scanning the incident wavelength from $\lambda_0 - x$ to $\lambda_0 + x$. Thus, a new resonant wavelength λ_1 is extracted, then the new scanning spectral range is modified to $\lambda_1 - x$ to $\lambda_1 + x$ (solid green straight line along the horizontal axis). If the RI continues to change from n_1 to n_2, the corresponding partial SPR plot (green solid curve) is then updated by scanning the incident wavelength from $\lambda_1 - x$ to $\lambda_1 + x$. This process will continue until the system has identified the next new resonant wavelength λ_2, which will trigger further modification of the scanning range, i.e., from $\lambda_2 - x$ to $\lambda_2 + x$. In a more general representation, the $i+1$'th scanning spectral range, which covers $\lambda_{i+1} - x$ to $\lambda_{i+1} + x$ (solid yellow straight line along the horizontal axis), is generated from the resonant wavelength extracted from the partial SPR plot near the SPR dip obtained in the i'th scanning spectral range of $\lambda_i - x$ to $\lambda_i + x$ (solid black straight line along horizontal axis). For a 2-D sensor array, a number of different resonant wavelengths will be obtained from the sensor elements as each of them has been designated to perform a specific sensing task. In such a situation, our system will try to cover the entire range of all the elements by registering the lower and upper limits, i.e., $\lambda_{i\ \mathrm{min}}$ and $\lambda_{i\ \mathrm{max}}$, of the spectral dip, and the range will become $\lambda_{i\ \mathrm{min}} - x$ to $\lambda_{i\ \mathrm{max}} + x$.

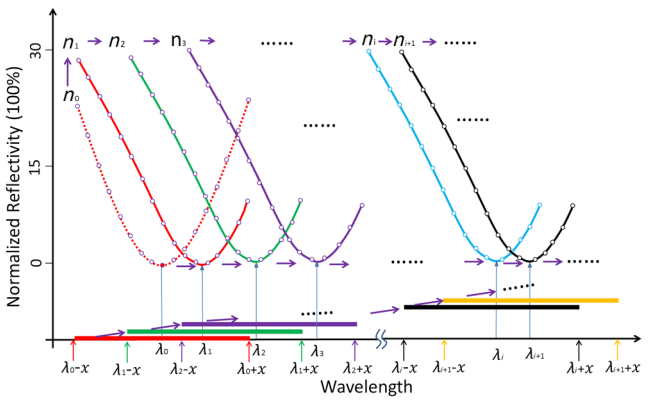

Fig. 3 Schematic showing the tracking of SPR dip movement based on the feedback loop technique. Here, $n_0, n_1, \ldots, n_i$, and n_{i+1} represent a series of RI values at the Au/sample interface when a molecular binding interaction is taking place on the sensor surface. When the RI changes continuously from n_0 to n_i, the spectral range to be scanned will also be adjusted automatically from the original spectral range $[\lambda_0 - x, \lambda_0 + x]$ to $[\lambda_i - x, \lambda_i + x]$ as guided by the feedback loop. This way, only a selected range around the resonance dip will be interrogated at all time, thereby drastically shortening the time to calculate the location of the SPR dip.

3 Results and Discussion

3.1 *Linearity and Resolution of Surface Plasmon Resonance Measurement*

To estimate the performance of our SPRi system, we measured the RI values of different salt-water mixtures. Salt solutions with a concentration level ranging from 0% to 25% in increments of 5% by volume, which corresponds to a RI ranging from 1.3330 to 1.3793 RIU,[26] were prepared. In the experiment, an incident angle of 72.5 deg in the prism was chosen based on the theoretical simulation of the SPR angular dip of water. The scanning spectral range was about 40 nm, and the time for finding the minima of the spectral SPR dip was about 4 s. The 3×3 array sensor sites, which were uniformly distributed on the chip, were spectrally monitored simultaneously to assess the performance of our system. The step changes of resonant wavelength obtained from different salt concentrations are shown in Fig. 4(a), and the corresponding shifts in spectral SPR dip, as caused by changes in RI, are shown in Fig. 4(b). Based on measurement data obtained in the wavelength range from 600 to 700 nm, the calculated resolution is 5.87×10^{-6} RIU, and the measured dynamic range of the system is 4.63×10^{-2} RIU. Here, the conversion from the minimum measurable wavelength shift to the corresponding change in refraction index value is performed with the equation $\sigma_{\mathrm{RI}} = \frac{\delta n}{\delta \lambda} \cdot \sigma_{\mathrm{SD}}$,[26] where σ_{RI} is the RI resolution, δn is the RI change of a bulk medium, $\delta\lambda$ is the calculated wavelength shift, and σ_{SD} is the estimated wavelength noise. Here, $\sigma_{\mathrm{SD}} = 0.034$ nm is obtained through averaging 10 measurements of the RMS noise of our system.

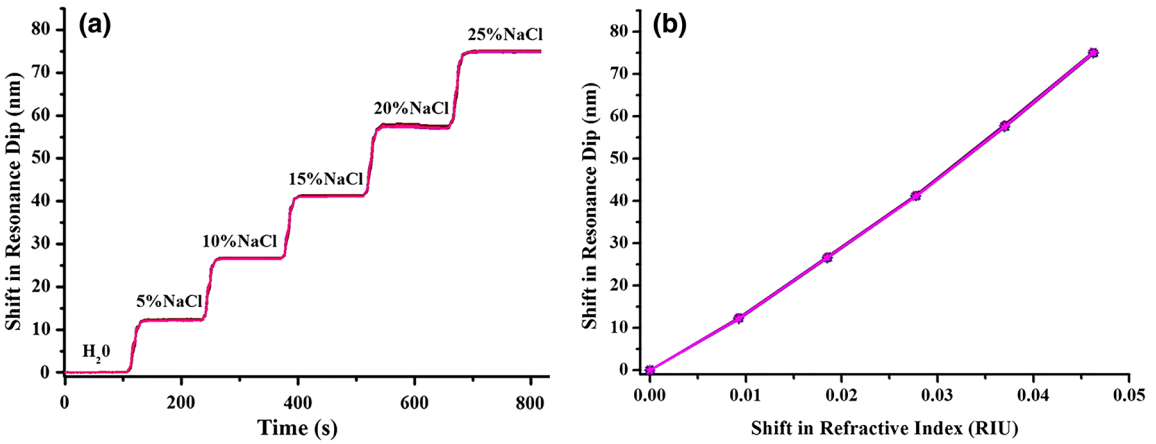

Fig. 4 (a) Shift of SPR dip versus salt concentration in water as detected by sensor sites within the 3×3 array. (b) Relationship between resonant wavelength of the SPR dip and the shift in RI as detected by the 3×3 array on the SPR chip. Each data point is obtained by averaging the intensity values of 30×20 pixels to reduce the effect of noise with no compromise in spatial resolution.

3.2 *Application to IgG Interaction Monitoring*

To assess the capability of our SPRi system for monitoring biomolecular interactions, we performed real-time monitoring of binding interactions between goat antirabbit IgG and rabbit IgG at different concentration levels. Rabbit IgG was dissolved in the array-spotting buffer at concentrations of 50, 100, 150, and 250 $\mu g\,ml^{-1}$. BSA was chosen as the positive control protein. A 3×5 array of protein dots was spotted on the SPR chip by hand. Within each column, the three spots had the same solution. The first column on the left was 100 $\mu g\,ml^{-1}$ BSA solution; other columns were rabbit IgG solution with concentrations of 250, 150, 100, and 50 $\mu g\,ml^{-1}$, from left to right [see Fig. 5(a)]. The diameter of the spots was about 1 mm, and the distance between the centers of the two adjacent spots was about 2.5 mm.

The IgG interaction procedures were carried out as follows. First, a 3×5 array chip was attached to the coupling prism using a small drop of RI matching liquid. A piece of molded PDMS was placed over the chip to form a sealed flow cell of 15 mm $\times$ 15 mm $\times$ 0.3 mm ($l \times w \times h$). We designed software to analyze the 15 sensing regions captured by the CCD. A set of 15 spectral SPR plots representing the binding interactions taking place on the spotted sensing regions were generated from the sensor chip. We manually tuned the incidence angle to achieve minimum intensity at the SPR dip for a phosphate buffer saline (PBS) sample. A glycine solution (100 mM, pH = 2.0) was injected for 5 min to regenerate the sensor surface. Next, a buffer solution, PBS 1×, was injected in the flow cell for 3 min with a micropump operating at a speed of 25 $\mu l/$ min to obtain a steady baseline. The initial small scanning range was set at $\lambda_{0\,min} - 20$ nm to $\lambda_{0\,max} + 20$ nm, in which $\lambda_{0\,min}$ and $\lambda_{0\,max}$ were, respectively, the minimum wavelength and maximum wavelength among the resonant wavelengths extracted from all the SPR spectral profiles obtained from the sensing regions. The half width of the scanning spectral range $x = 20$ nm was chosen to achieve the fastest wavelength interrogation and lowest noise. After obtaining a steady baseline for several minutes, the process of capturing the SPR image was automatically executed for one scan to obtain the baseline spectral SPR image, which was produced through extracting the spectral SPR plot of individual sensor sites. Then IgG solutions of 5, 10, and 15 $\mu g\,ml^{-1}$ were in turn pumped into the sensor chip. The subsequent antigen–antibody binding interaction taking place on the detection surface was monitored in real time, as shown in Fig. 5. The binding interaction measurement time was typically ~3 min for each concentration with a constant flow of sample using a syringe pump. After completion of each binding interaction measurement, PBS 1× solution was pumped into the flow chamber for 2 min to ensure adequate buffer washing. To see clearly the shift of the SPR wavelength dip as a function of protein concentration, we arranged the SPR plots into three groups corresponding to the upper, middle, and lower rows of the 3×5 array. Each group included five members corresponding to four different concentration levels each of IgG and the BSA control sample. As shown in Figs. 5(b)–5(d), the first group showed that the shift of the SPR wavelength dip increases as protein concentration increases in the range from 5 to 15 $\mu g\,ml^{-1}$. Locations on the other two groups on the chip exhibited a similar trend. After completing buffer washing and regeneration steps, the system collects a steady baseline image using data gathered for 3 min, and a reference SPR dip image is produced. Consequently, a reference SPR dip images is available for each IgG concentration. All subsequent SPR dip images obtained while binding interactions were ongoing were analyzed and compared using the first set of reference images and the updated one as the shift of the SPR dip progressed. Figures 5(e)–5(g) show representative images of SPR shift obtained with different protein concentration levels. In the images, the left column of sensor sites shows no change because goat antirabbit IgG does not specifically bind to BSA. In images of other sensor sites, the presence of binding interactions as the SPR dips shift continuously is clearly revealed: the wavelength shift is approximately proportional to the change in concentration of the protein solution.

3.3 *Determination of Important Parameters*

Within our SPRi technique, interrogation speed is determined by the choice of parameters including step size and total spectral

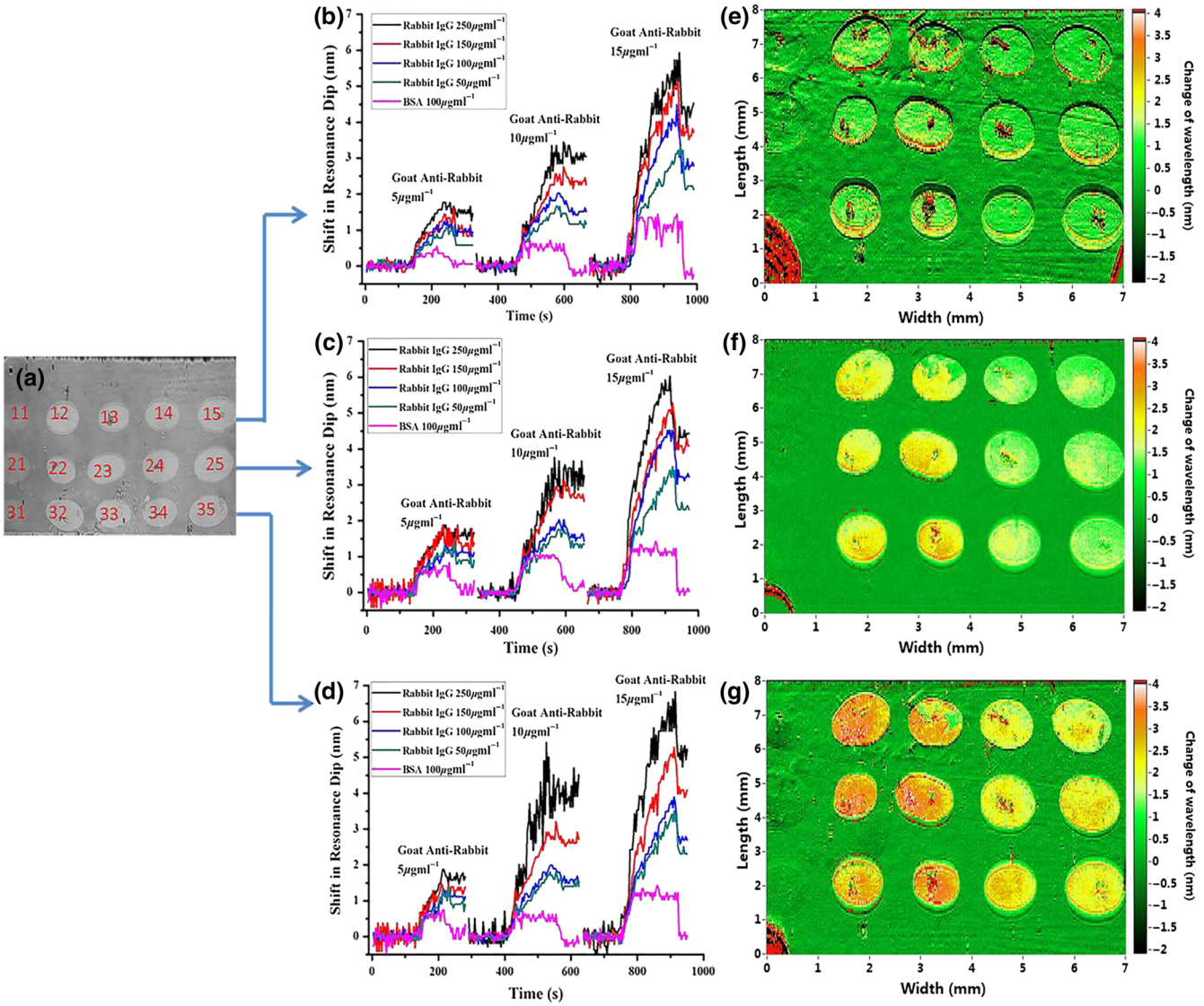

Fig. 5 Measurement of goat antirabbit IgG and rabbit IgG antigen–antibody interaction. (a) White light image of the SPR sensor chip, (b–d) real-time wavelength response of antigen–antibody binding interactions, (e–g) SPR shift images of a 3×5 array obtained after interaction with goat antirabbit IgG solutions of 5, 10, and 15 μg ml^{-1}, respectively. The first column sensor sites, respectively, marked by 11, 21, 31 corresponding to 100 μg ml^{-1} BSA; the second column sites are, respectively, marked by 12, 22, 32, which correspond to 250 μg ml^{-1} rabbit IgG; the third, fourth, and fifth column sites are marked by 13, 23, 33, and 14, 24, 34 and 15, 25, 35, which correspond to 150, 100, and 50 μg ml^{-1} rabbit IgG, respectively. The color of individual SPR plot, i.e., pink, green, blue, red or black, denotes the probe area of i_1, i_2, i_3, i_4, or i_5, respectively.

width to be scanned. We analyzed the effects of step size and spectral width on system noise by measuring the variations in SPR dip obtained from pure water. As shown in Fig. 6, for a given step size, system noise decreased and reached a constant level as spectral width increased. Conversely, decreasing the step size decreased the system noise, and the overall interrogation time also increased. For our antigen–antibody interaction experiment, a spectral width of 40 nm and a step size of 1 nm were chosen because they provide optimal performance in terms of noise and interrogation speed under normal curve fitting situations. The salt solution experiment showed that our spectral SPR technique could monitor binding interactions at a rate of about 4 s per data point with an RI resolution and dynamic range similar to that of traditional spectral SPR technique.

Spatial resolution is also an important parameter of the SPR imaging system. It primarily defines the density of the final sensor array. We measured the spatial resolution of our SPR imaging system using a standard resolution target. The x-axis and y-axis resolution limits are 27.8 and 35.8 μm, which, respectively, correspond to 6 and 4 pixels of the CCD imaging chip. In our experiments, a 3×2 pixel area was averaged to improve the signal-to-noise ratio in the process of producing the SPR image. But for all SPR plots, a larger area, i.e., 30×20 pixels square, was used to obtain the SPR plots for the binding interaction to achieve an optimized signal-to-noise ratio.

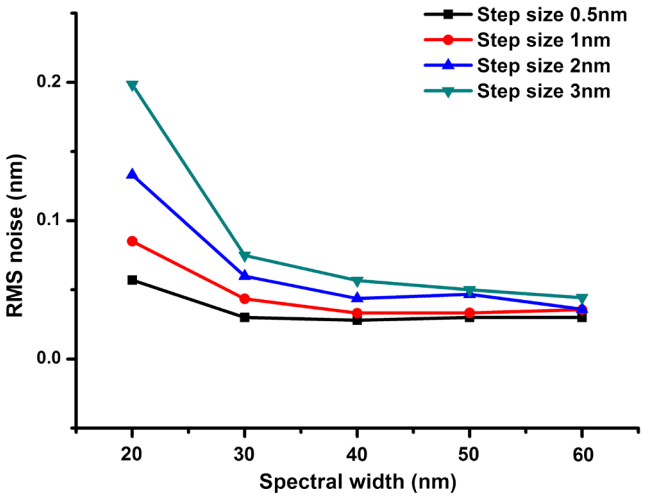

Fig. 6 Root-mean-square (RMS) noise level versus scanning spectral width for different step sizes.

4 Conclusion

We have demonstrated a fast wavelength-scanned SPR imaging technique with no mechanical moving parts. By incorporating a feedback loop in the LCTF scanning algorithm, we have drastically reduced measurement time for obtaining spectral SPR dips from a 2-D array. The key function of the feedback loop is to actively follow the movement of the SPR dip while the binding interaction is ongoing so that there is no need to perform wavelength sweeping over an unnecessarily wide spectral range. Compared to the 2-D wavelength-scanning SPR imaging techniques reported in the literature, the proposed spectral SPR sensor has the greatest potential for true real-time label-free monitoring of molecular interactions.[18,27,28] Moreover, the detection speed can be further improved, e.g., by increasing the scanning wavelength step, decreasing the scanning wavelength range, or using the five-parameter fitting algorithm.[11] Therefore, it is possible for our SPR imaging technology to simultaneously measure the interactions at every spot of a microarray with real-time imaging of the sensor surface. In our experiments, the RI resolution has yet to be better than that of the single wavelength SPR sensor;[19,29] this is mainly because the LCTF used in our experiment has a bandpass spectral width of 10 nm. Another source of system noise is not having a precise collimation beam. The angle of the beam divergence decreases the resolution of our SPR system. In the future, we can improve the RI resolution by using a singular value decomposition or minimum hunting method[19] or replacing the LCTF with one that offers narrower bandpass width.

Disclosures

No conflicts of interest, financial or otherwise, are declared by the authors.

Acknowledgments

This work has been partially supported by the National Major Scientific Research Instruments and Equipment Development Project from National Natural Science Foundation of China (Grant No. 61527827); National Basic Research Program of China (Grant No. 2015CB352005); Guangdong Natural Science Foundation (Grant No. 2014A030312008); Guangdong Province Project (Grant Nos. 2015KGJHZ002 and 2015A020214023); Shenzhen Science and Technology R&D Foundation (Grant No. JCYJ20160422151611496); Collaborative Research Fund (CRF) (Grant No. CUHK1/CRF/12G) from the Hong Kong Research Grants Council, Innovation and Technology Fund (ITF) (Grant No. GHP/014/13SZ) from the Hong Kong Innovation and Technology Commission.

References

1. V. Chabot et al., "Biosensing based on surface plasmon resonance and living cells," *Biosens. Bioelectron.* **24**(6), 1667–1673 (2009).
2. J. Homola, "Surface plasmon resonance sensors for detection of chemical and biological species," *Chem. Rev.* **108**(2), 462–493 (2008).
3. V. G. Shah et al., "Calibration-free concentration analysis of protein biomarkers in human serum using surface plasmon resonance," *Talanta* **144**, 801–808 (2015).
4. C. L. Wong and M. Olivo, "Surface plasmon resonance imaging sensors: a review," *Plasmonics* **9**(4), 809–824 (2014).
5. B. P. Nelson et al., "Surface plasmon resonance imaging measurements of DNA and RNA hybridization adsorption onto DNA microarrays," *Anal. Chem.* **73**(22), 1–7 (2001).
6. M. Piliarik and J. Homola, "Surface plasmon resonance (SPR) sensors: approaching their limits?," *Opt. Express* **17**(19), 16505–16517 (2009).
7. S. Scarano et al., "Surface plasmon resonance imaging for affinity-based biosensors," *Biosens. Bioelectron.* **25**(5), 957–966 (2010).
8. A. Sereda et al., "Compact 5-LEDs illumination system for multispectral surface plasmon resonance sensing," *Sens. Actuators B* **209**, 208–211 (2015).
9. Y. Shao et al., "Wavelength-multiplexing phase-sensitive surface plasmon imaging sensor," *Opt. Lett.* **38**(9), 1370–1372 (2013).
10. W. Knoll, "Interfaces and thin films as seen by bound electromagnetic waves," *Annu. Rev. Phys. Chem.* **49**, 569–638 (1998).
11. A. Sereda et al., "High performance multi-spectral interrogation for surface plasmon resonance imaging sensors," *Biosens. Bioelectron.* **54**, 175–180 (2014).
12. J. B. Beusink et al., "Angle-scanning SPR imaging for detection of biomolecular interactions on microarrays," *Biosens. Bioelectron.* **23**(6), 839–844 (2008).
13. L. Liu et al., "Parallel scan spectral surface plasmon resonance imaging," *Appl. Opt.* **47**(30), 5616–5621 (2008).
14. B. K. Singh and A. C. Hillier, "Multicolor surface plasmon resonance imaging of ink jet-printed protein microarrays," *Anal. Chem.* **79**(14), 5124–5132 (2007).
15. G. D. VanWiggeren et al., "A novel optical method providing for high-sensitivity and high-throughput biomolecular interaction analysis," *Sens. Actuators B* **127**(2), 341–349 (2007).
16. N. S. Eum et al., "Variable wavelength surface plasmon resonance (SPR) in biosensing," *Biosystems* **98**(1), 51–55 (2009).
17. J. Homola et al., "Spectral surface plasmon resonance biosensor for detection of staphylococcal enterotoxin B in milk," *Int. J. Food Microbiol.* **75**, 61–69 (2002).
18. J. S. Yuk et al., "Analysis of protein interactions on protein arrays by a wavelength interrogation-based surface plasmon resonance biosensor," *Proteomics* **4**(11), 3468–3476 (2004).
19. O. R. Bolduc, L. S. Live, and J. F. Masson, "High-resolution surface plasmon resonance sensors based on a dove prism," *Talanta* **77**(5), 1680–1687 (2009).
20. B. Sutapun et al., "A multichannel surface plasmon resonance sensor using a new spectral readout system without moving optics," *Sens. Actuators B* **156**, 312–318 (2011).
21. C. J. Alleyne et al., "Analysis of surface plasmon spectro-angular reflectance spectrum: real-time measurement, resolution limits, and applications to biosensing," *Opt. Lett.* **36**(1), 46–48 (2011).
22. F. Bardin et al., "Surface plasmon resonance spectro-imaging sensor and associated data processing for biomolecular surface interaction characterization," *Proc. SPIE* **6450**, 64500N (2007).
23. S. Otsuki and M. Ishikawa, "Wavelength-scanning surface plasmon resonance imaging for label-free multiplexed protein microarray assay," *Biosens. Bioelectron.* **26**(1), 202–206 (2010).

24. J. A. Ruemmele et al., "A localized surface plasmon resonance imaging instrument for multiplexed biosensing," *Anal. Chem.* **85**(9), 4560–4566 (2013).
25. M. Palumbo et al., "A single chip multi-channel surface plasmon resonance imaging system," *Sens. Actuators B Chem.* **90**, 264–270 (2003).
26. S. P. Ng et al., "White-light spectral interferometry for surface plasmon resonance sensing applications," *Opt. Express* **19**(5), 4521–4527 (2011).
27. F. Bardin et al., "Surface plasmon resonance spectro-imaging sensor for biomolecular surface interaction characterization," *Biosens. Bioelectron.* **24**(7), 2100–2105 (2009).
28. L. Liu et al., "A two-dimensional polarization interferometry based parallel scan angular surface plasmon resonance biosensor," *Rev. Sci. Instrum.* **82**(2), 023109 (2011).
29. A. Abbas, M. J. Linman, and Q. Cheng, "New trends in instrumental design for surface plasmon resonance-based biosensors," *Biosens. Bioelectron.* **26**(5), 1815–1824 (2011).

Kaiqiang Chen graduated with a BEng degree from Huazhong University of Science and Technology Wenhua College. Currently, he is an MEng student in the College of Optoelectronics Engineering, Shenzhen University. His research mainly involves the development of surface resonance sensors for biomedical applications.

Youjun Zeng was awarded a BSc degree from Changchun University of Science and Technology. He is currently an MEng student in the College of Optoelectronics Engineering, Shenzhen University. His research focuses on surface resonance imaging technique.

Lei Wang was awarded a BSc degree from Changchun University of Science and Technology. He is currently an MEng student in the College of Optoelectronics Engineering, Shenzhen University. His research focuses on surface resonance imaging technique.

Dayong Gu earned his MD degree from Third Military Medical University. Currently, he is a senior researcher at Central Laboratory of Health Quarantine, Shenzhen International Travel Health Care Center, Shenzhen Entry-Exit Inspection and Quarantine Bureau, China. His research interests include microbial molecular diagnostic techniques and optical biosensors.

Jianan He received his PhD in the College of Engineering at Peking University in 2011. He is an associate professor of Shenzhen Entry-Exit inspection and Quarantine Bureau. He was a postdoctoral fellow at Peking University from 2011 to 2013. His research focuses on biosensors, particularly development of chemical surface for biomedical and infectious disease diagnostics applications.

Shu-Yuen Wu received his BSc and MPhil degrees in applied physics from The City University of Hong Kong. He continued to study electronic engineering and received his PhD at The Chinese University of Hong Kong. He is working on biosensing systems related to surface plasmon resonance, laboratory on a disk (LOAD) system, nanoparticles, and nanoislands.

Ho-Pui Ho received his BEng and PhD degrees in electrical and electronic engineering from the University of Nottingham. His academic interests include nanosized semiconductor materials for photonic and sensor applications, optical instrumentation, surface plasmon resonance biosensors, lab-on-a-chip, and biophotonics. He has published over 270 peer-reviewed articles, and holds 15 Chinese and 5 US patents. He is a fellow of SPIE and HKIE, and a senior member of IEEE.

Xuejin Li received his PhD in physical electronics from Tianjin University in 2005. He developed his interest in fiber optic sensor technologies, their principles and applications. He now works as the director of the Shenzhen Key Laboratory of Sensor Technology and Shenzhen Engineering Laboratory for Optical Fiber Sensors and Networks, Shenzhen University. He was awarded the Outstanding Scholar of Shenzhen University in 2013. He has published over 80 papers.

Junle Qu received his PhD in 1998 from Xi'an Institute of Optics and Precision Mechanics, Chinese Academy of Sciences. He is currently a professor of optical engineering at Shenzhen University. His research interests include nonlinear optical microscopy, fluorescence lifetime imaging and super-resolution optical imaging. He published over 120 papers in peer-reviewed journals and holds 20 patents. He is a senior member of SPIE and the Chinese Optical Society (COS), and the director of COS Biomedical Photonics Committee.

Bruce Zhi Gao received his BS and MS degrees, respectively, in optoelectronics in 1985 and applied laser physics in 1988, both from Tianjin University, China. He received his PhD in biomedical engineering from the University of Miami in 1999, then followed a 3-year postdoctoral training in cell and tissue engineering at the University of Minnesota. He is currently a professor and the director of the biophotonics lab in the Department of Bioengineering at Clemson University.

Yonghong Shao obtained his PhD in optics from Changchun Institute of Optics, Fine Mechanics, and Physics, Chinese Academy of Science, China. Currently, he is a professor at Key Laboratory of Optoelectronic Devices and Systems of Ministry of Education and Guangdong Province, Shenzhen University. His research interests involve surface plasmon resonance sensors, multiphoton fluorescence microscopy and confocal endoscopy. He has published over 40 papers and 17 Chinese patents.